Inorganic Chemistry

pubs.acs.org/IC

Article

Efficient Broadband Near-Infrared $CaMgGe_2O_6:Cr^{3+}$ Phosphor for pc-LED

Limin Fang, Liangliang Zhang,* Hao Wu, Huajun Wu, Guohui Pan, Zhendong Hao, Feng Liu,* and Jiahua Zhang*

Cite This: *Inorg. Chem.* 2022, 61, 8815−8822

Read Online

ACCESS | Metrics & More | Article Recommendations | Supporting Information

ABSTRACT: Broadband near-infrared (NIR) phosphor-converted light-emitting diodes (pc-LEDs) are essential to integrate near-infrared spectrometers into mobile devices for the rapid and noninvasive detection of biological components. However, efficient broadband NIR phosphors with a peak emission wavelength longer than 800 nm are deficient. In this study, $CaMgGe_2O_6:Cr^{3+}$ phosphor was prepared by a high-temperature solid-state reaction. The phosphor doped with $0.02Cr^{3+}$ showed an emission band at 845 nm with a broad bandwidth of 160 nm and a high quantum yield of 84% under 450 nm excitation. The broadband NIR pc-LED was fabricated using $CaMgGe_2O_6:0.02Cr^{3+}$ phosphor based on a blue light-emitting diode (LED) chip. A photoelectric efficiency of 27.2% @ 10 mA and an NIR output power of 57.98 mW @ 100 mA were achieved, which are the highest values reported yet for broadband NIR pc-LEDs with a peak wavelength longer than 800 nm. Using the fabricated NIR pc-LED as the light source, the characteristic absorption spectra of some substances were obtained. All of the results indicated that the $CaMgGe_2O_6:Cr^{3+}$ phosphor has considerable potential in near-infrared spectroscopic applications.

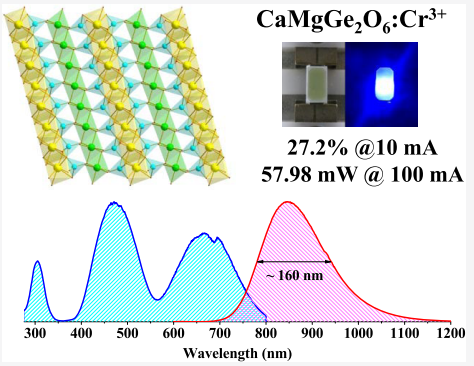

INTRODUCTION

Near-infrared spectroscopy (NIRS) is a simple, rapid, and noninvasive method for the detection of biological components. The absorption of overtone and combination bands of fundamental molecular vibrations just occur in the near-infrared spectral region. Therefore, the absorption of molecular compounds is as unique as a fingerprint. The novel NIR phosphor-converted light-emitting diode (NIR pc-LED) light source makes it possible to integrate a near-infrared spectrometer into mobile devices such as smartphones and tablets due to its compact size, low power consumption, and high vibration resistance. Thus, the NIRS technology can be extended to the consumer end of food, agriculture, and biomedicine.[1−3] NIR pc-LEDs are composed of broadband near-infrared phosphor and high-efficiency blue LED chips; therefore, an appropriate broadband near-infrared phosphor is the key to its light source performance.

The Cr^{3+} ion with an electronic configuration of $3d^3$ is an ideal activating ion for broadband near-infrared phosphor because the position and bandwidth of NIR emission originating from $^4T_2 \rightarrow {}^4A_1$ can change considerably under the influence of a crystal-field environment, and the excitation band originating from $^4A_1 \rightarrow {}^4T_1(^4F)$ matches well with a high-efficiency blue LED chip. In the last few years, a number of Cr^{3+}-doped NIR phosphors have been reported, some of which can achieve high efficiency, but most of them have an emission wavelength shorter than 800 nm or a full width at half-maximum (FWHM) less than 150 nm.[4−14] Highly efficient NIR pc-LEDs with an emission wavelength longer than 800 nm are rarely reported[15−25] for several reasons: first, this kind of pc-LED has a larger blue-to-NIR optical conversion loss; second, high-efficiency phosphors that meet the spectral profile requirements are deficient; lastly, target phosphors usually show poor thermal stability due to a larger Stokes shift and strong electron−phonon coupling. When the emission wavelength of Cr^{3+}-doped near-infrared phosphor shifts in the long-wave direction, its broadband near-infrared emission will cover more areas of the near-infrared spectrum. Therefore, there is significant demand for long-wave light sources in the application of near-infrared spectroscopy. A feasible solution is to actively seek new materials that meet the application requirements.

Germanate-based host materials can provide a weaker crystal-field environment for Cr^{3+} ions as compared with the corresponding silicate-based host materials; therefore, germanate-based Cr^{3+}-doped phosphors are more likely to achieve long-wavelength emission. In this work, Cr^{3+}-activated

Received: March 10, 2022
Published: June 1, 2022

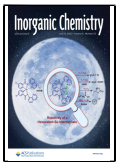

https://doi.org/10.1021/acs.inorgchem.2c00798
Inorg. Chem. 2022, 61, 8815−8822

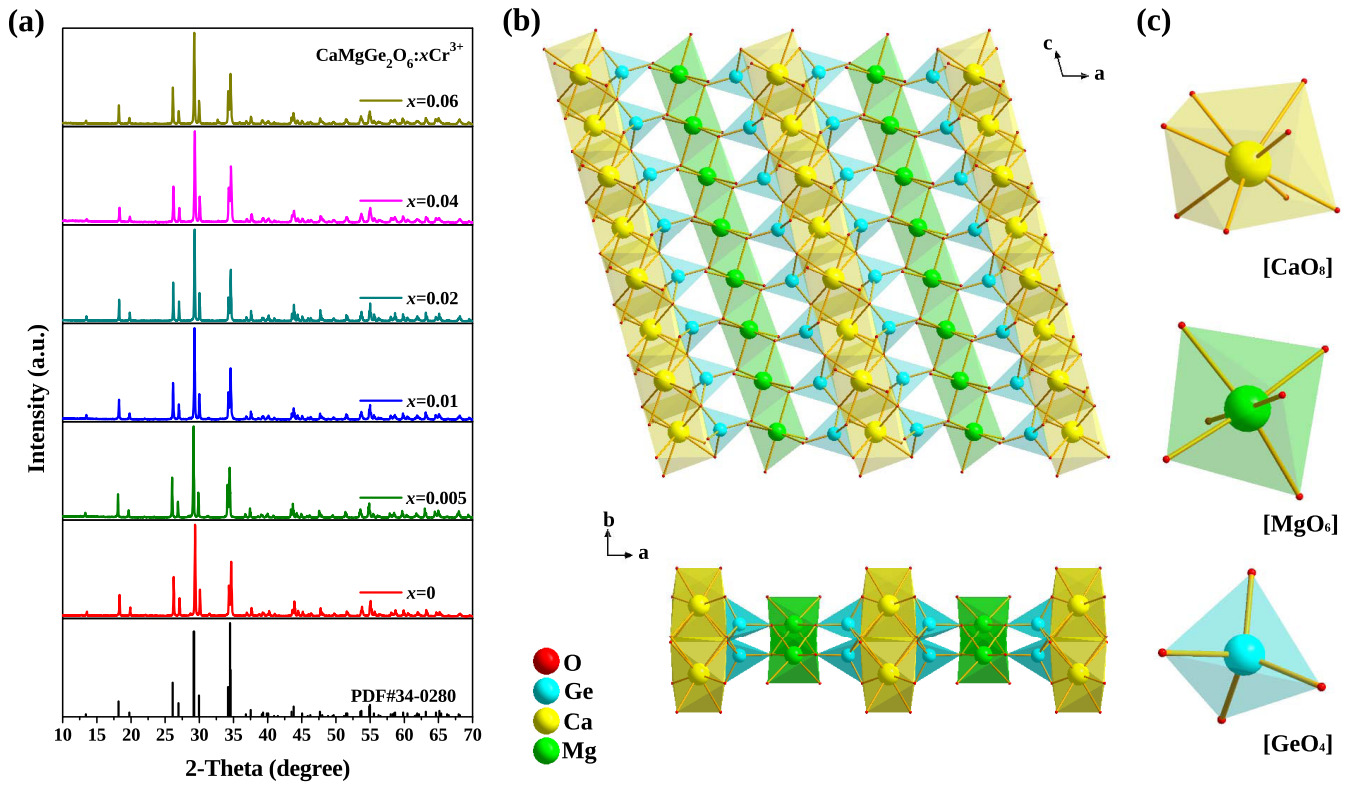

Figure 1. (a) XRD patterns of $CaMgGe_2O_6$:xCr^{3+}; (b) crystal structure of $CaMgGe_2O_6$; (c) coordination of cations.

$CaMgGe_2O_6$ broadband NIR phosphors were synthesized by a high-temperature solid-state reaction. Upon 450 nm blue-light excitation, $CaMgGe_2O_6$:$0.02Cr^{3+}$ shows an emission band at 845 nm, with an FWHM of 160 nm. The internal and external quantum efficiencies upon 450 nm excitation were 84 and 30%, respectively. NIR pc-LEDs were fabricated using $CaMgGe_2O_6$:$0.02Cr^{3+}$ phosphors and blue LED chips. A photoelectric efficiency of 27.2% @ 10 mA current and an NIR output of 57.98 mW @ 100 mA were achieved.

MATERIALS AND METHODS

Preparation of $CaMgGe_2O_6$:xCr^{3+} Phosphors. Powder samples of $CaMg_{1-x}Ge_2O_6$:xCr^{3+} (abbreviated to $CaMgGe_2O_6$:xCr^{3+} hereafter) were synthesized via a high-temperature solid-state reaction using stoichiometric mixtures of $CaCO_3$ (99%), MgO (98%), GeO_2 (99.999%), and Cr_2O_3 (99.95%) as raw materials and 0.06 mole ratio of NaCl (99.8%) as the flux and charge compensator. After grinding thoroughly with ethyl alcohol in a mortar, the powdered mixture was transferred into a corundum crucible and sintered in a muffle furnace. The temperature was first increased to 900 °C, maintained for 60 min, then increased to 1250 °C, and sintered for 240 min. The sintering process was carried out in an air atmosphere.

Sample Characterization. The crystal structure of these as-prepared phosphors was examined using a D8 Focus powder X-ray diffractometer (Bruker, Germany).

Room-temperature photoluminescence excitation spectra were measured by an FLS920 fluorescence spectrophotometer (Edinburgh Instrument, U.K.) equipped with a 150 W Xe lamp as the excitation source. Room-temperature photoluminescence spectra were obtained by combining the results of the FLS920 fluorescence spectrophotometer and a HAAS2000 photoelectric measuring system (EVERFINE, China). All photodetectors were calibrated with an HL-3 VIS–NIR light source (Ocean Optics) beforehand. Diffuse reflection spectra were recorded using a UV-3600 plus UV–Vis–NIR spectrometer (Shimadzu, Japan).

The quantum efficiency was measured using the Quantaurus-QY Plus C13534-12 absolute photoluminescence (PL) quantum yield measurement system (Hamamatsu Photonics).

The fluorescence decay curves of the $CaMgGe_2O_6$:Cr^{3+} samples were measured using a TRIAX 550 spectrometer. The electric signal was recorded by a Tektronix digital oscilloscope. Pulsed laser from an optical parametric oscillator was used as the excitation source.

The temperature-dependent emission spectra were measured using a THMS600E cooling–heating platform (Linkam Scientific Instruments, U.K.) and a QEPro microfiber spectrometer (Ocean Optics). A 450 nm laser diode was used as the excitation source.

NIR pc-LEDs were fabricated by combining the $CaMgGe_2O_6$:$0.02Cr^{3+}$ phosphors with a 450 nm InGaN LED chip. The adhesive was an epoxy resin with the same weight as that of the phosphor. The photoelectric properties of the blue InGaN LED chip and pc-LEDs were measured using the HAAS 2000 photoelectric measuring system.

RESULTS AND DISCUSSION

Structural Analysis of $CaMgGe_2O_6$:xCr^{3+} Phosphors. Figure 1a shows the powder XRD patterns of $CaMgGe_2O_6$:xCr^{3+} and the standard card of $CaMgGe_2O_6$ (PDF #34-0280). Well-assigned diffraction peaks indicate the successful synthesis of $CaMgGe_2O_6$ phosphors. The crystalline structure of $CaMgGe_2O_6$ is similar to that of monoclinic pyroxene, and it belongs to the space group $C2/c$ (15). The structure of $CaMgGe_2O_6$ is composed of $[CaO_8]$ dodecahedrons, $[MgO_6]$ octahedrons, and $[GeO_4]$ tetrahedrons. Each type of polyhedron is connected by shared oxygen atoms to form an infinite chain parallel to the c-axis as shown in Figure 1b,c. Considering the ionic radii of Ca^{2+} (1.12 Å, coordination number (CN) = 8), Mg^{2+} (0.72 Å, CN = 6), Ge^{4+} (0.39, Å CN = 4), Na^{+} (1.18 Å, CN = 8), and Cr^{3+} (0.615 Å, CN = 6),[26] Na^{+} was the closest to Cr^{2+} and Cr^{3+} closest to Mg^{2+} in terms of their ionic radii. Therefore, Na^{+} should enter Ca^{2+} sites and

https://doi.org/10.1021/acs.inorgchem.2c00798
Inorg. Chem. 2022, 61, 8815–8822

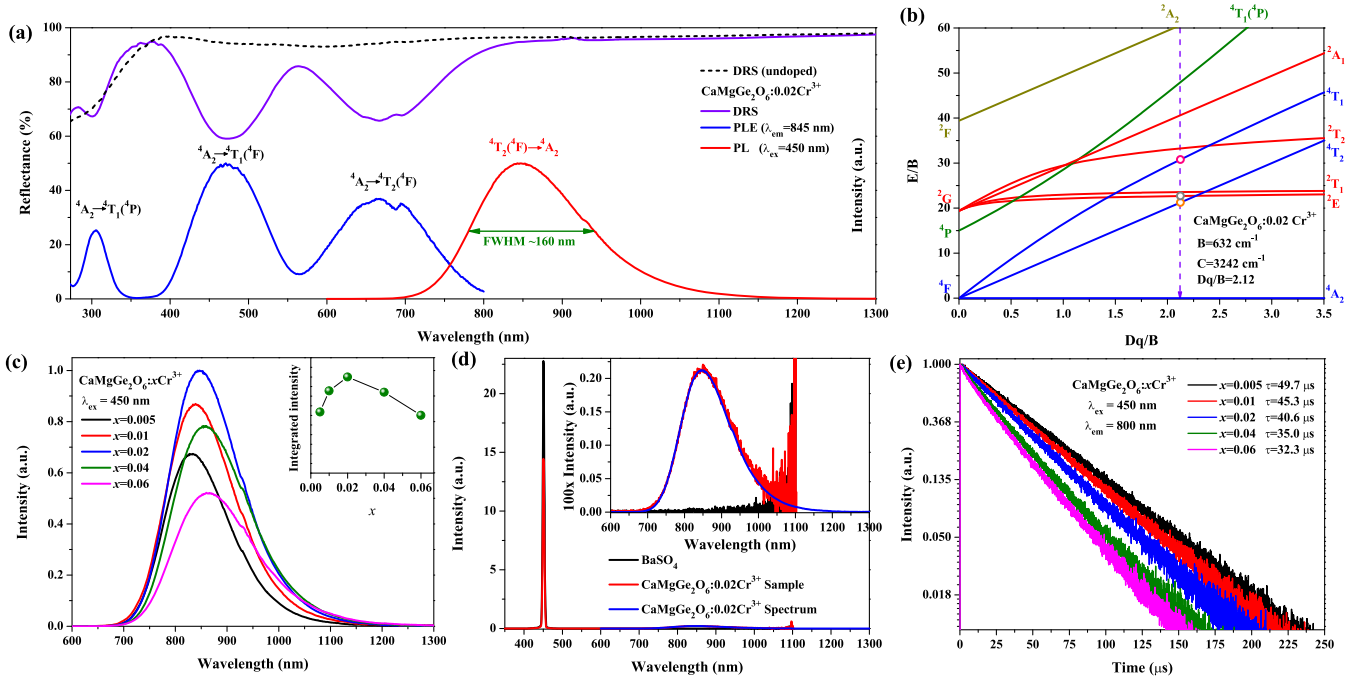

Figure 2. (a) Diffuse reflectance spectra, normalized excitation spectra, and emission spectra of $CaMgGe_2O_6$:0.02Cr^{3+} at room temperature; (b) Tanabe−Sugano diagram of $CaMgGe_2O_6$:0.02Cr^{3+} and zero phonon line (ZPL) energies of $^4T_1$, $^4T_2$, and ^2E energy levels of $CaMgGe_2O_6$:0.02Cr^{3+}; (c) integrated intensity of NIR emission under 450 nm excitation; (d) measured PL spectra with $BaSiO_4$ as the reference for the quantum efficiency measurement of $CaMgGe_2O_6$:0.02Cr^{3+}; (e) fluorescence decay of $CaMgGe_2O_6$:$x$$Cr^{3+}$.

form a charge compensation relationship with Cr^{3+} and Mg^{2+}. Furthermore, the crystal-field stabilization energy (CFSE) refers to the energy difference between the electron configuration of the specific ligand field and the isotropic field. The CFSE is large for ions with an electronic configuration of d^3 and d^8 ions in the octahedral ligand, resulting in the Cr^{3+} site preferring octahedral sites.[27,28] Thus, we believe that Cr^{3+} ions substitute for Mg^{2+} to form $[CrO_6]$ octahedrons.

Photoluminescence Properties. The diffuse reflectance spectra (DRS), excitation spectra, and emission spectra of $CaMgGe_2O_6$:0.02Cr^{3+} at room temperature are shown in Figure 2a. The diffuse reflectance spectra correspond to the excitation spectra monitored at 845 nm. The characteristic absorption peak $^4T_1 \rightarrow {}^4T_3$ of Cr^{4+} transition was around 1100 nm; there was no absorption peak of Cr^{4+} in the DRS of the $CaMgGe_2O_6$:0.02Cr^{3+} sample. Both the diffuse reflectance spectra and the excitation spectra contained three excitation bands originating from spin-allowed transitions of Cr^{3+}: they are excitation bands centered at 305, 475, and 666 nm corresponding to $^4A_2 \rightarrow {}^4T_1(^4P)$, $^4A_2 \rightarrow {}^4T_1(^4F)$, and $^4A_2 \rightarrow {}^4T_2(^4F)$ transitions of Cr^{3+}, respectively. In addition, the excitation peaks originating from the spin-forbidden $^4A_2 \rightarrow {}^2E$ transition can be found at 697 nm. Under the excitation of a 450 nm blue light, the phosphors exhibit a broadband emission at 845 nm with an FWHM of 160 nm, which correspond to $^4T_2(^4F) \rightarrow {}^4A_2$ spin-allowed transitions of Cr^{3+}.

Combined with the spectral data mentioned above, zero phonon line (ZPL) positions of ^2E and $^4T_2$ energy levels of $CaMgGe_2O_6$:0.02Cr^{3+} can be given directly by the following equation, and then the crystal-field parameters can be estimated:

$$E_{ZPL} = \frac{1}{2}(E_{PLE} + E_{PL}) \tag{1}$$

where E_{PLE} and E_{PL} represent energies corresponding to the positions of the excitation peak and emission peak of the specified energy level, respectively. The Cr^{3+} ion has an electron configuration of d^3. According to the theory of Tanabe, Sugano, and Henderson, the zero phonon line positions of $^4T_1$ and $^4T_2$ energy levels are as follows:[29,30]

$$E(^4T_1) = \frac{15}{2}B + 15D_q - \frac{\sqrt{5}}{2}(45B^2 - 36D_qB + 20D_q^2)^{1/2} \tag{2}$$

$$E(^4T_2) = 10D_q \tag{3}$$

There is an approximate relation for the zero phonon line position of the ^2E energy level.[31,32]

$$E_{ZPL}(^2E) \approx 3.05C + 7.9B - 1.8\left(\frac{B^2}{D_q}\right) \tag{4}$$

where B and C are the Racah repulsion parameters and D_q is the cubic crystal-field parameter. It is generally accepted that the Stokes shifts of $^4T_1$ and $^4T_2$ energy levels are very close; hence, we take the crystal-field parameters when they are equal.[33] The Tanabe−Sugano diagram of $CaMgGe_2O_6$:Cr can be drawn using the calculated crystal-field parameters and Anselmoo's program,[34] as shown in Figure 2b. The zero phonon line positions of $^4T_1$, $^4T_2$, and ^2E energy levels of $CaMgGe_2O_6$:0.02Cr^{3+} are marked in the Tanabe−Sugano diagram. Detailed data are listed in Tables S1−S3.

The emission integral intensity of $CaMgGe_2O_6$:$x$$Cr^{3+}$ reached the maximum when the Cr^{3+}-doping concentration was 0.02, as shown in Figure 2c. The quantum efficiency (QE)

https://doi.org/10.1021/acs.inorgchem.2c00798
Inorg. Chem. 2022, 61, 8815−8822

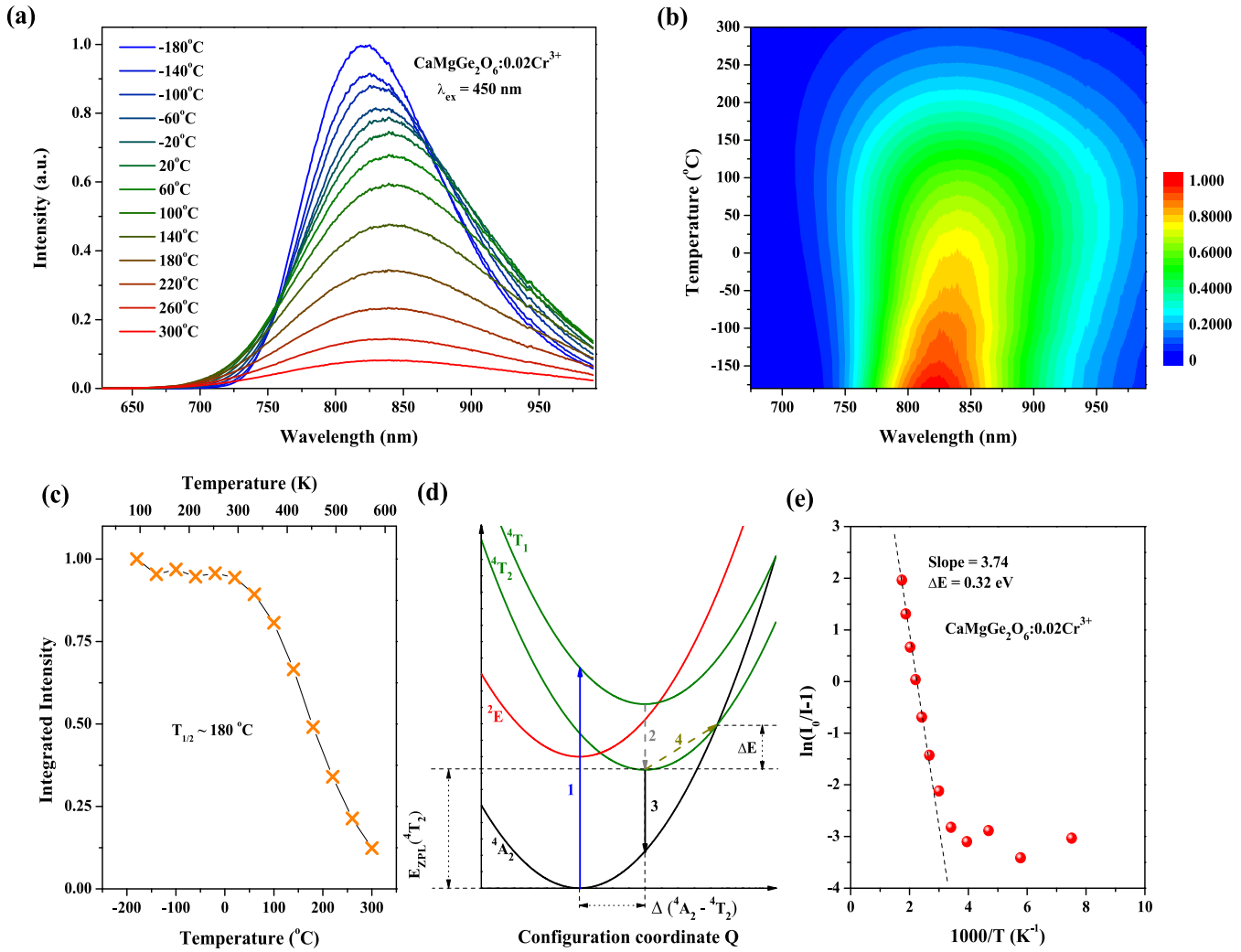

Figure 3. (a) Temperature-dependent emission spectra of $CaMgGe_2O_6$:0.02Cr^{3+}; (b) two-dimensional (2D) color map of the temperature-dependent emission spectra of $CaMgGe_2O_6$:0.02Cr^{3+}; (c) temperature-dependent normalized integrated emission intensities of $CaMgGe_2O_6$:0.02Cr^{3+}; (d) schematic configuration coordinate diagram of Cr^{3+}; (e) $\ln(I_0/I - 1)$ vs $1/T$ plots of $CaMgGe_2O_6$:0.02Cr^{3+}.

Table 1. Efficiencies and Thermal Stabilities of Some Cr^{3+} Singly Doped Phosphors with Wavelengths Longer than 800 nm and their pc-LEDs

materials	λ_{em} (nm)	FWHM (nm)	IQE [%]	$\eta_{pc\text{-}LED}$ [%]	$T_{1/2}$ [°C]	pc-LED NIR output [mW]	refs
$CaMgGe_2O_6$:0.02 Cr^{3+}	845	160	84	27.2 @ 10 mA	180	57.98 @ 100 mA	this work
$LiInSi_2O_6$:Cr^{3+}	840	143	~75	~23 @ 10 mA	~220	54.60 @ 100 mA	4
$LiScGe_2O_6$:Cr^{3+}	886	160	72.6	14.95 @ 20 mA	~127	407.3 @ 300 mA	25
$CaMgSi_2O_6$:0.04Cr^{3+}	821	187	45.9	11.6 @ 10 mA	236	23.73 @ 100 mA	24
$LiInGe_2O_6$:Cr^{3+}	880	172	81.2		~105		15
$InBO_3$:Cr^{3+}	820	138	46.3	~12.5 @ 20 mA	~150	37.50 @ 120 mA	17
$Sr_9Ga_{0.2}(PO_4)_7$:0.7Cr^{3+}	850	~150	66.3	12.34 @ 20 mA	~77	19.79 @ 150 mA	22
$LiScP_2O_7$:0.06Cr^{3+}	880	170	38.0	~10 @ 20 mA	~85	19.00 @ 100 mA	23
Ga_4GeO_8:0.02Cr^{3+}	850	215	60	~10.5 @ 10 mA	~170	56 @ 400 mA	16
$Mg_3Ga_2GeO_8$:Cr^{3+}	~800	244		8.5 @ 60 mA		6.14 @ 60 mA	19
$La_3Ga_5GeO_{14}$:Cr^{3+}	780, 920	330				18.20 @ 350 mA	18

of $CaMgGe_2O_6$:0.02Cr^{3+} was measured, and the measured spectra are shown in Figure 2d. Accordingly, the internal quantum efficiency (IQE) and external quantum efficiency (EQE) upon 450 nm excitation were calculated to be 84 and 30%, respectively. The fluorescence decay curve of $CaMgGe_2O_6$:$x$$Cr^{3+}$ at room temperature monitored at 800 nm with a 450 nm pulse excitation is shown in Figure 2e. It can be seen that with the increase of x from 0.005 to 0.06, the lifetime values of Cr^{3+} are shortened from 49.7 to 32.3 μs due to concentration quenching. As shown in Figure S2, the decay curves of $CaMgGe_2O_6$:0.02Cr^{3+} are fitted well by a single-exponential function.

Temperature-Dependent Emission Spectra. Considering that the pc-LED chips work at high temperatures,

https://doi.org/10.1021/acs.inorgchem.2c00798
Inorg. Chem. 2022, 61, 8815−8822

temperature-dependent emission spectra of $CaMgGe_2O_6$:0.02Cr^{3+} from −180 °C (93 K) to 300 °C (573 K) were recorded and are shown Figure 3a,b. The emission spectra broaden and red shift obviously with an increase in the temperature. The FWHM value increases from ∼148 nm at −180 °C to ∼196 nm at 300 °C. Figure 3c displays the integrated emission intensities of $CaMgGe_2O_6$:xCr^{3+} as a function of temperature. Below 20 °C (293 K), the integrated emission intensities hardly change; above this temperature, the integrated intensities decrease. The thermal-quenching temperature ($T_{1/2}$) of the $CaMgGe_2O_6$:0.02Cr^{3+} sample was about 180 °C (453 K). The thermal stability of $CaMgGe_2O_6$:0.02Cr^{3+} phosphor is relatively high compared with that of other singly doped long-wavelength emission NIR phosphors listed in Table 1.

As shown in Figure 3d, after blue-light excitation (process 1), the electrons will relax from the $^4T_1(^4F)$ to the $^4T_2(^4F)$ level (process 2) and then return to the ground state through radiative transition (process 3). The thermal characteristics come from the nonradiative transition caused by multiphonon relaxation at the cross-point of the $^4A_2$ ground level and $^4T_2$ excited level (process 4). Then, the thermal characteristics of these luminescent materials can be determined using the following formula[14]

$$I(T) = \frac{I_0}{1 + A \times e^{(-\Delta E/k \times T)}} \quad (5)$$

where $I(T)$ is the integrated intensity at a certain temperature, I_0 is the initial integrated intensity, and k is the Boltzmann constant. Taking $1/T$ as the abscissa and $\ln(I_0/I - 1)$ as the ordinate, the thermal activation energy ΔE was estimated to be 0.32 eV by fitting the slope of the curve, as shown in Figure 3e.

Application to NIR pc-LEDs. The NIR pc-LEDs were fabricated using $CaMgGe_2O_6$:0.02Cr^{3+} phosphors with a 450 nm InGaN chip. Figure 4a shows the luminescence spectra of our NIR pc-LED under different drive currents and its photographs. It can be seen that as the drive current increased from 10 to 200 mA, the NIR luminescence spectral profile of the NIR pc-LED device did not change, except for the increase in intensity. The NIR output power (600−1100 nm) and photoelectric efficiency (electricity to NIR light) are displayed in Figure 4b; the near-infrared light output power can reach 57.98 mW @ 100 mA, with a bandwidth of 160 nm. A photoelectric efficiency of 27.2% @ 10 mA current and 12.9% @ 200 mA current can be achieved. It can be seen that the electricity-to-NIR power conversion efficiency of the pc-LED decreases considerably with the increase in the driving current. However, a large part of this efficiency drop arises due to the decline of efficiency of the 450 nm LED chip itself. Figure S3 shows the luminescence spectra, blue-light power output, and electricity-to-blue light conversion efficiency of the 450 nm LED chip for packaging under different driving currents. According to these data, we can estimate the blue-to-NIR optical quantum conversion efficiency QE_{O-O} of a pc-LED. As shown in Figure 4b and Table S4, the blue-to-NIR QE_{O-O} of a pc-LED @ 10 mA is 70.4%, which is higher than the EQE value of $CaMgGe_2O_6$:0.02Cr^{3+} phosphor. as displayed in Figure 2d. This is attributed to the internal reflection of blue light in the pc-LED, which enhances the blue-light absorption of the phosphor.[13] Only about 17% of the blue-to-NIR optical quantum conversion efficiency is lost due to the thermal quenching of the NIR phosphor as the driving current increases from 10 to 200 mA. This result indicates that the thermal stability of the $CaMgGe_2O_6$:0.02Cr^{3+} phosphor is acceptable in pc-LED applications. Therefore, the photoelectric efficiency of the fabricated pc-LED under a low drive current can better reflect the efficiency level of a phosphor. For a comparison, several Cr^{3+} singly doped phosphors with emission wavelengths longer than 800 nm are listed in Table 1. As can be seen, the photoelectric efficiency of 27.2% @ 10 mA current of the pc-LED fabricated by our phosphors ranks high among long-wavelength NIR pc-LEDs.

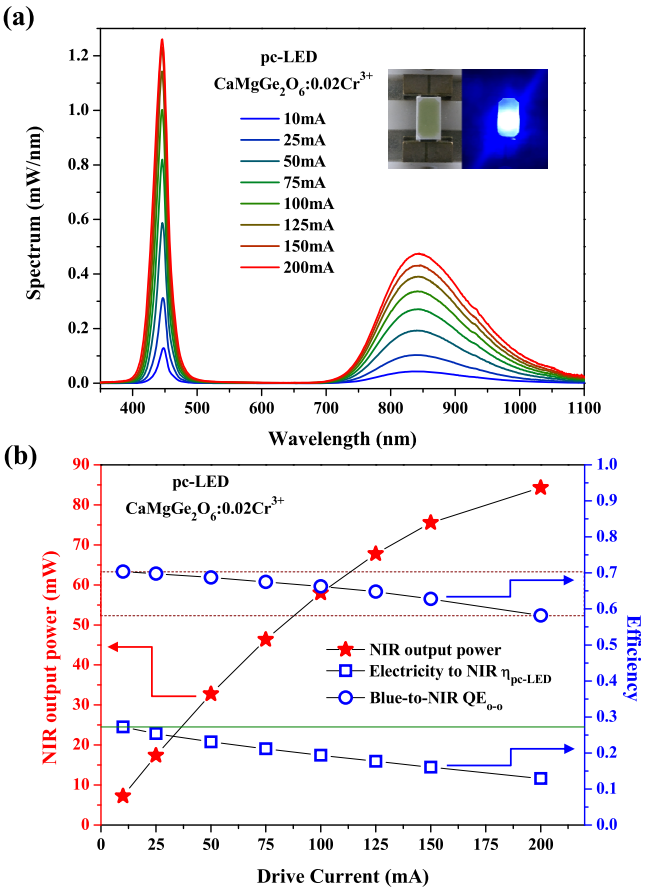

Figure 4. (a) Luminescence spectra of NIR pc-LEDs fabricated with $CaMgGe_2O_6$:0.02 Cr^{3+} (insets are the photographs of NIR pc-LEDs); (b) NIR output power (650−1100 nm), photoelectric efficiency, and optical conversion efficiency of the NIR pc-LEDs.

To demonstrate the application prospects of $CaMgGe_2O_6$:Cr^{3+} phosphors in NIR spectroscopy for substance measurements, water (H_2O), cyclohexane (C_6H_{12}), alcohol (C_2H_5OH), and acetic acid (CH_3COOH) were selected as substances to be analyzed. The NIR pc-LED fabricated with $CaMgGe_2O_6$:0.02Cr^{3+} was used as the light source of the self-built NIR transmission spectrum measurement system. The experimental setup is shown in Figure S4. The NIR transmission spectra of the corresponding substances are shown in Figure 5a, with the transmission spectra of an empty centrifuge tube for a comparison. The calculated absorbance spectra of the corresponding substances are shown in Figure 5b: each substance shows its characteristic absorption in the 700−1100 nm region. For example, the absorption peak at 970 nm of the water sample was attributed to the first and second overtones of the O−H stretching $2\nu_1 + \nu_3$, where ν_1 and ν_3 are different vibrational modes of water molecules; absorption peaks at 923 and 933 nm of the cyclohexane sample

https://doi.org/10.1021/acs.inorgchem.2c00798
Inorg. Chem. 2022, 61, 8815−8822

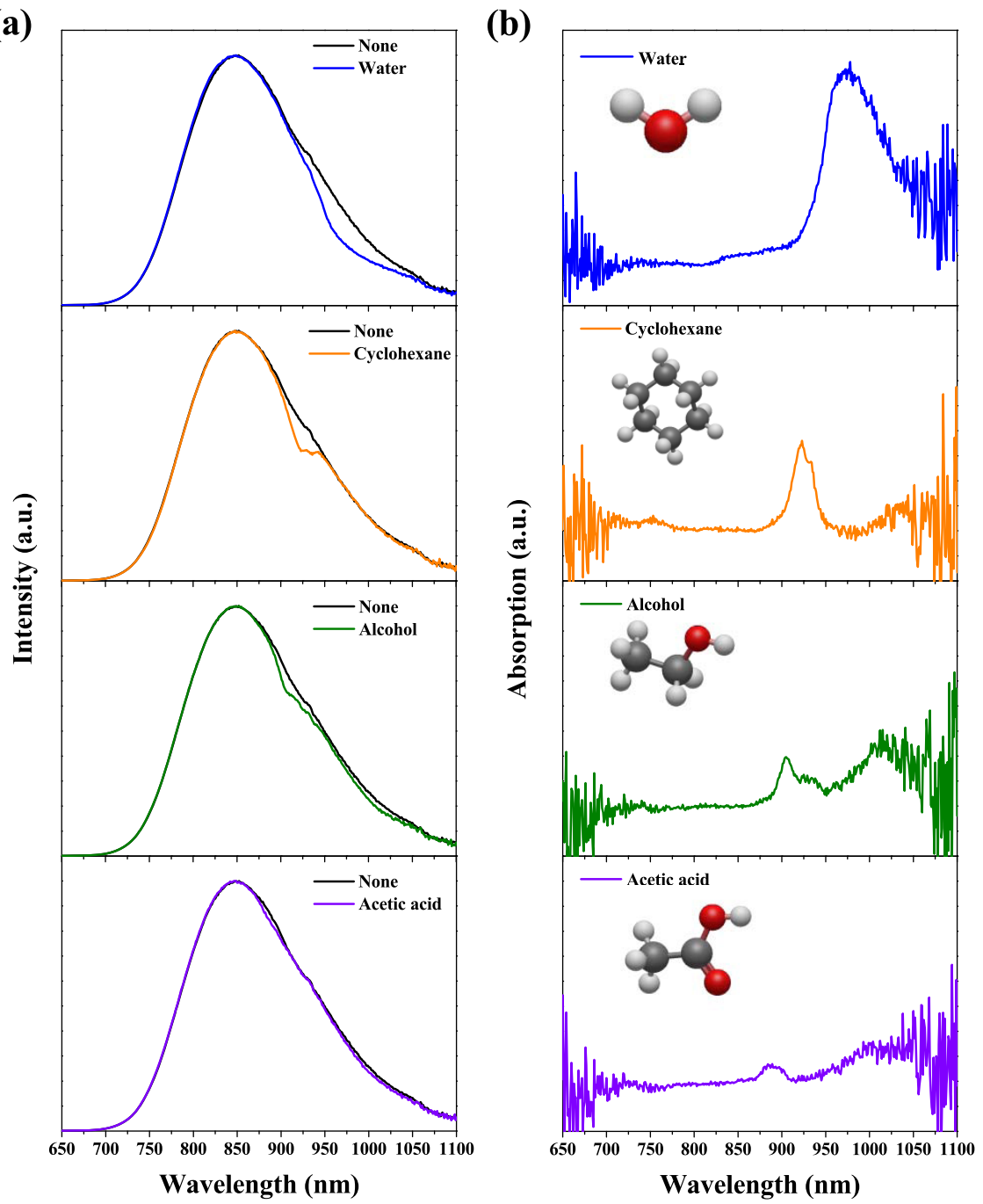

Figure 5. (a) Transmission spectra of NIR light after penetrating water, cyclohexane, alcohol, and acetic acid, respectively; (b) calculated absorbance spectra of the corresponding substances; optical density = $-\log(I/I_0)$.

correspond to the third overtone of the antisymmetric CH_2 stretching normal modes $3\nu_a$,[35] and so on. In the calculated absorption spectrum, the signal noise before 700 nm is caused by the weak emission intensity of the NIR pc-LED in the spectral region, whereas the signal noise after 1050 nm is caused by the decrease in the sensitivity of the detector in the spectral region. Overall, the near-infrared absorption spectra obtained from the experiment are satisfactory. These results further show the feasibility of our phosphors in the field of nondestructive testing.

CONCLUSIONS

In general, Cr^{3+}-doped $CaMgGe_2O_6$ broadband near-infrared phosphors were prepared. The optimal sample, $CaMgGe_2O_6$:$0.02Cr^{3+}$, under blue-light excitation, shows an emission band at 845 nm with an FWHM of 160 nm. The internal and external quantum efficiencies upon 450 nm excitation are 84 and 30%, respectively. The fabricated NIR pc-LEDs achieved a photoelectric efficiency of 27.2% @ 10 mA current and an NIR output of 57.98 mW @ 100 mA. These results suggest that $CaMgGe_2O_6$:Cr phosphors have considerable potential for applications in NIR pc-LEDs.

https://doi.org/10.1021/acs.inorgchem.2c00798
Inorg. Chem. 2022, 61, 8815−8822

■ ASSOCIATED CONTENT

Supporting Information

The Supporting Information is available free of charge at https://pubs.acs.org/doi/10.1021/acs.inorgchem.2c00798.

Possible ion radii of $CaMgGe_2O_6$:Cr; spectacular data of $CaMgGe_2O_6$:0.02Cr^{3+}; crystal-field parameters of $CaMgGe_2O_6$:0.02Cr^{3+}; zero phonon line positions of $^4T_1$, $^4T_2$, and ^2E energy levels of $CaMgGe_2O_6$:0.02Cr^{3+} in the Tanabe-Sugano diagram; fluorescence decay of $CaMgGe_2O_6$:0.02Cr^{3+}; luminescence spectra of the blue LED chip; output power and photoelectric efficiency of the 450 nm LED chip; drive current, voltage, output power, and efficiencies of the blue LED chip and NIR pc-LED; photographs of the experimental setup; spectra of NIR light after penetrating an empty 10 mL centrifuge and the calculated absorption spectra (PDF)

■ AUTHOR INFORMATION

Corresponding Authors

Liangliang Zhang − *State Key Laboratory of Luminescence and Applications, Changchun Institute of Optics, Fine Mechanics and Physics, Chinese Academy of Sciences, Changchun 130033, P. R. China;* orcid.org/0000-0002-9546-8786; Email: zhangliangliang@ciomp.ac.cn

Feng Liu − *Key Laboratory for UV-Emitting Materials and Technology of Ministry of Education, Northeast Normal University, Changchun 130024, P. R. China;* orcid.org/0000-0002-7310-8763; Email: fengliu@nenu.edu.cn

Jiahua Zhang − *State Key Laboratory of Luminescence and Applications, Changchun Institute of Optics, Fine Mechanics and Physics, Chinese Academy of Sciences, Changchun 130033, P. R. China; Center of Materials Science and Optoelectronic Engineering, University of Chinese Academy of Sciences, Beijing 100049, P. R. China;* orcid.org/0000-0001-5180-7267; Email: zhangjh@ciomp.ac.cn

Authors

Limin Fang − *State Key Laboratory of Luminescence and Applications, Changchun Institute of Optics, Fine Mechanics and Physics, Chinese Academy of Sciences, Changchun 130033, P. R. China; Center of Materials Science and Optoelectronic Engineering, University of Chinese Academy of Sciences, Beijing 100049, P. R. China;* orcid.org/0000-0001-7089-3383

Hao Wu − *State Key Laboratory of Luminescence and Applications, Changchun Institute of Optics, Fine Mechanics and Physics, Chinese Academy of Sciences, Changchun 130033, P. R. China;* orcid.org/0000-0002-8396-7393

Huajun Wu − *State Key Laboratory of Luminescence and Applications, Changchun Institute of Optics, Fine Mechanics and Physics, Chinese Academy of Sciences, Changchun 130033, P. R. China*

Guohui Pan − *State Key Laboratory of Luminescence and Applications, Changchun Institute of Optics, Fine Mechanics and Physics, Chinese Academy of Sciences, Changchun 130033, P. R. China;* orcid.org/0000-0002-2190-2690

Zhendong Hao − *State Key Laboratory of Luminescence and Applications, Changchun Institute of Optics, Fine Mechanics and Physics, Chinese Academy of Sciences, Changchun 130033, P. R. China*

Complete contact information is available at: https://pubs.acs.org/10.1021/acs.inorgchem.2c00798

Notes

The authors declare no competing financial interest.

■ ACKNOWLEDGMENTS

This work was partially supported by the National Natural Science Foundation of China (Grant Nos. 52072361, 12074373, 11874055, 11974346, 11904361, 12074374, and 52102192), Youth Innovation Promotion Association CAS No. 2020222, Key Research and Development Program of Jilin province (20200401050GX, 20200401004GX, and 20210201024GX), the Opening Project Key Laboratory of Transparent Opto-functional Inorganic Material, Chinese Academy of Sciences.

■ REFERENCES

(1) Pasquini, C. Near infrared spectroscopy: A mature analytical technique with new perspectives − A review. *Anal. Chim. Acta* **2018**, *1026*, 8−36.

(2) Nicolaï, B. M.; Beullens, K.; Bobelyn, E.; Peirs, A.; Saeys, W.; Theron, K. I.; Lammertyn, J. Nondestructive measurement of fruit and vegetable quality by means of NIR spectroscopy: A review. *Postharvest Biol. Technol.* **2007**, *46*, 99−118.

(3) Mustafa, F. H.; Bek, E. J.; Huvanandana, J.; Jones, P. W.; Carberry, A. E.; Jeffery, H. E.; Jin, C. T.; McEwan, A. L. Length-free near infrared measurement of newborn malnutrition. *Sci. Rep.* **2016**, *6*, No. 36052.

(4) Xu, X.; Shao, Q.; Yao, L.; Dong, Y.; Jiang, J. Highly efficient and thermally stable Cr3+-activated silicate phosphors for broadband near-infrared LED applications. *Chem. Eng. J.* **2020**, *383*, No. 123108.

(5) Shao, Q.; Ding, H.; Yao, L.; Xu, J.; Liang, C.; Jiang, J. Photoluminescence properties of a ScBO3:Cr3+ phosphor and its applications for broadband near-infrared LEDs. *RSC Adv.* **2018**, *8*, 12035−12042.

(6) He, S.; Zhang, L.; Wu, H.; Wu, H.; Pan, G.; Hao, Z.; Zhang, X.; Zhang, L.; Zhang, H.; Zhang, J. Efficient super broadband NIR Ca2LuZr2Al3O12:Cr3+,Yb3+ Garnet phosphor for pc-LED light source toward NIR spectroscopy applications. *Adv. Opt. Mater.* **2020**, *8*, No. 1901684.

(7) Zhang, L.; Wang, D.; Hao, Z.; Zhang, X.; Pan, G.; Wu, H.; Zhang, J. Cr3+ -doped broadband NIR Garnet phosphor with enhanced luminescence and its application in NIR spectroscopy. *Adv. Opt. Mater.* **2019**, *7*, No. 1900185.

(8) Liu, S.; Wang, Z.; Cai, H.; Song, Z.; Liu, Q. Highly efficient near-infrared phosphor LaMgGa11O19:Cr3+. *Inorg. Chem. Front.* **2020**, *7*, 1467−1473.

(9) Jia, Z.; Yuan, C.; Liu, Y.; Wang, X.-J.; Sun, P.; Wang, L.; Jiang, H.; Jiang, J. Strategies to approach high performance in Cr3+-doped phosphors for high-power NIR-LED light sources. *Light: Sci. Appl.* **2020**, *9*, No. 86.

(10) Shi, M.; Yao, L.; Xu, J.; Liang, C.; Dong, Y.; Shao, Q. Far-red-emitting YAl3(BO3)4:Cr3+ phosphors with excellent thermal stability and high luminescent yield for plant growth LEDs. *J. Am. Ceram. Soc.* **2021**, *104*, 3279−3288.

(11) Zou, X.; Wang, X.; Zhang, H.; Kang, Y.; Yang, X.; Zhang, X.; Molokeev, M. S.; Lei, B. A highly efficient and suitable spectral profile Cr3+-doped garnet near-infrared emitting phosphor for regulating photomorphogenesis of plants. *Chem. Eng. J.* **2022**, *428*, No. 132003.

(12) Yu, D.; Zhou, Y.; Ma, C.; Melman, J. H.; Baroudi, K. M.; LaCapra, M.; Riman, R. E. Non-rare-earth Na3AlF6:Cr3+ phosphors for far-red light-emitting diodes. *ACS Appl. Electron. Mater.* **2019**, *1*, 2325−2333.

(13) Xiao, H.; Zhang, J.; Zhang, L.; Wu, H.; Wu, H.; Pan, G.; Liu, F.; Zhang, J. Cr3+ activated Garnet phosphor with efficient blue to far-red conversion for pc-LED. *Adv. Opt. Mater.* **2021**, *9*, No. 2101134.

(14) Nie, W.; Yao, L.; Chen, G.; Wu, S.; Liao, Z.; Han, L.; Ye, X. A novel Cr3+ -doped Lu2CaMg2Si3O12 garnet phosphor with

broadband emission for near-infrared applications. *Dalton Trans.* **2021**, *50*, 8446−8456.
(15) Liu, T.; Cai, H.; Mao, N.; Song, Z.; Liu, Q. Efficient near-infrared pyroxene phosphor LiInGe2O6:Cr3+ for NIR spectroscopy application. *J. Am. Ceram. Soc.* **2021**, *104*, 4577−4584.
(16) Yao, L.; Shao, Q.; Shi, M.; Shang, T.; Dong, Y.; Liang, C.; He, J.; Jiang, J. Efficient ultra-broadband Ga4GeO8:Cr3+ phosphors with tunable peak wavelengths from 835 to 980 nm for NIR pc-LED application. *Adv. Opt. Mater.* **2021**, *10*, No. 2102229.
(17) Sun, Z.; Ning, Q.; Zhou, W.; Luo, J.; Chen, P.; Zhou, L.; Pang, Q.; Zhang, X. Structural and spectroscopic investigation of an efficient and broadband NIR phosphor InBO3:Cr3+ and its application in NIR pc-LEDs. *Ceram. Int.* **2021**, *47*, 13598−13603.
(18) Rajendran, V.; Fang, M.-H.; Guzman, G. N. D.; Lesniewski, T.; Mahlik, S.; Grinberg, M.; Leniec, G.; Kaczmarek, S. M.; Lin, Y.-S.; Lu, K.-M.; Lin, C.-M.; Chang, H.; Hu, S.-F.; Liu, R.-S. Super broadband near-infrared phosphors with high radiant flux as future light sources for spectroscopy applications. *ACS Energy Lett.* **2018**, *3*, 2679−2684.
(19) Dai, D.; Wang, Z.; Xing, Z.; Li, X.; Liu, C.; Zhang, L.; Yang, Z.; Li, P. Broad band emission near-infrared material Mg3Ga2-GeO8:Cr3+: Substitution of Ga-In, structural modification, luminescence property and application for high efficiency LED. *J. Alloys Compd.* **2019**, *806*, 926−938.
(20) Zhou, X.; Geng, W.; Li, J.; Wang, Y.; Ding, J.; Wang, Y. An ultraviolet−visible and near-infrared-responded broadband NIR phosphor and its NIR spectroscopy application. *Adv. Opt. Mater.* **2020**, *8*, No. 1902003.
(21) Wu, J.; Huang, D.; Liang, S.; Xu, S.; Zhu, H. Photoluminescence properties and device performance of Cr3+, Yb3+ Co-doped LaSc3(BO3)4 near infrared phosphors. *Chin. J. Lumin.* **2021**, *42*, 793−803.
(22) Zhao, F.; Cai, H.; Song, Z.; Liu, Q. Structural confinement for Cr3+ activators toward efficient near-infrared phosphors with suppressed concentration quenching. *Chem. Mater.* **2021**, *33*, 3621−3630.
(23) Yao, L.; Shao, Q.; Han, S.; Liang, C.; He, J.; Jiang, J. Enhancing near-infrared photoluminescence intensity and spectral properties in Yb3+ Codoped LiScP2O7:Cr3+. *Chem. Mater.* **2020**, *32*, 2430−2439.
(24) Fang, L.; Hao, Z.; Zhang, L.; Wu, H.; Wu, H.; Pan, G.; Zhang, J. Cr3+-doped broadband near infrared diopside phosphor for NIR pc-LED. *Mater. Res. Bull.* **2022**, *149*, No. 111725.
(25) Chen, X. H.; Song, E. H.; Zhou, Y. Y.; He, F. Q.; Yang, J. Q.; Zhang, Q. Y. Distorted octahedral site occupation-induced high-efficiency broadband near-infrared emission in LiScGe2O6:Cr 3+ phosphor. *J. Mater. Chem. C* **2021**, *9*, 13640−13646.
(26) Shannon, R. D. Revised effective ionic radii and systematic studies of interatomic distances in halides and chalcogenides. *Acta Crystallogr., Sect. A* **1976**, *32*, 751−767.
(27) Akasaka, M.; Takasu, Y.; Handa, M.; Nagashima, M.; Hamada, M.; Ejima, T. Distribution of Cr 3+ between octahedral and tetrahedral sites in synthetic blue and green (CaMgSi2O6)95 (CaCrAlSiO6)5 diopsides. *Mineral. Mag.* **2019**, *83*, 497−505.
(28) Ikeda, K.; Yagi, K. Crystal-field spectra for blue and green diopsides synthesized in the join CaMgSi2O6-CaCrAlSiO6. *Contrib. Mineral. Petrol.* **1982**, *81*, 113−118.
(29) Tanabe, Y.; Sugano, S. On the absorption spectra of complex ions. I. *J. Phys. Soc. Jpn.* **1954**, *9*, 753−766.
(30) Adachi, S. Photoluminescence spectroscopy and crystal-field parameters of Cr 3+ ion in red and deep red-emitting phosphors. *ECS J. Solid State Sci. Technol.* **2019**, *8*, R164−R168.
(31) Henderson, B.; Marshall, A.; Yamaga, M.; O'Donnell, K. P.; Cockayne, B. The temperature dependence of Cr 3+ photoluminescence in some garnet crystals. *J. Phys. C: Solid State Phys.* **1988**, *21*, 6187−6198.
(32) Malysa, B.; Meijerink, A.; Jüstel, T. Temperature dependent Cr3+ photoluminescence in garnets of the type X3Sc2Ga3O12 (X = Lu, Y, Gd, La). *J. Lumin.* **2018**, *202*, 523−531.
(33) Struve, B.; Huber, G. The effect of the crystal field strength on the optical spectra of Cr3+ in gallium garnet laser crystals. *Appl. Phys. B* **1985**, *36*, 195−201.
(34) *Anselmoo Python-solver for Tanabe-Sugano and energy-correlation diagrams*. https://github.com/Anselmoo/TanabeSugano, 2021.
(35) Workman, Jerry., Jr.; Weyer, L. *Practical Guide to Interpretive Near-Infrared Spectroscopy*, 1st ed.; CRC Press, 2007.

https://doi.org/10.1021/acs.inorgchem.2c00798
Inorg. Chem. 2022, 61, 8815−8822